Machine Learning Assisted Caching and Adaptive LDPC Coded Modulation for Next Generation Wireless Communications

Hassan Nooh, Zhikun Zhu and Soon Xin Ng
School of Electronics and Computer Science, University of Southampton, SO17 1BJ, U.K.

http://www.wireless.ecs.soton.ac.uk

Keywords: Low Density Parity-check Codes, Latent Dirichlet Allocation, Adaptive Modulation and Coding, K-Means Clustering.

Abstract: Unmanned Aerial Vehicles (UAVs) constitute a key technology for next generation wireless communications. Compared to terrestrial communications, wireless systems with low-altitude UAVs are in general faster to deploy, more flexible and are likely to have better communication channels due to the presence of short-range Line of Sight (LoS) links. In this contribution, a Latent Dirichlet Allocation (LDA) based machine learning algorithm was utilized to optimize the content caching of UAVs, while the K-means clustering algorithm was invoked for optimizing the assignment of mobile users to the UAVs. We further investigated a practical adaptive Low Density Parity Check (LDPC) coded modulation (ALDPC-CM) scheme for the communication links between the UAVs and the users. We found that the caching efficiency of each UAV can be boosted from 50% with random caching to above 90% with the employment of LDA. We also found that the proposed ALDPC-CM scheme is capable of performing closely to the ideal perfect coding based scheme, where the mean delay of the former is only about 0.05 ms higher than that of the latter, when the UAV system aims to minimize both the transmission and request delays.

1 INTRODUCTION

Emerging technologies such as Internet of Things (IoT) and autonomous vehicles are expected to be commercialized as their performance requirements are theoretically met by 5G specifications (Americas, 2018). Various methods of deployment and system architectures have been proposed, yet a clear all-round approach has not been found. Unmanned Aerial Vehicles (UAVs), also referred to as drones, have been massively employed in various applications during the past several decades (Valavanis and Vachtsevanos, 2014), especially for military and recreational use. More specifically, UAVs have been used mainly for military purposes due to its high cost. However, continuous development has made it possible to build low-cost and light-weight UAVs for civil and commercial applications. UAV based wireless communication seems to be a promising solution to support connectivity for users outside the infrastructure coverage (Merwaday and Guvenc, 2015), which may be caused by disasters, shadowing or overloading. Besides, UAVs can relay the blocked signals from the base station (BS) to users due to its advantage in mobility and flexibility (Zeng et al., 2016). In cellular networks, each BS covers and serves a specific region. In order to extend the coverage area of the BS, the concept of Remote Radio Head (RRH) has been investigated (Chen et al., 2017). RRH is a transceiver that is connected to a BS via the wireless or wired interface. Therefore, RRH can be regarded as a relay node between the BS and the users. In this contribution, UAVs are employed as our RRHs.

On the other hand, each UAV can be equipped with limited memory to cache useful contents for future user requests, in order to improve the Quality of Service (QoS). This is referred to as mobile edge caching (Wang et al., 2017) and machine learning algorithms could be employed to predict user requests and to perform caching updates. We model the user preference as a multinomial process based on the Latent Dirichlet Allocation (LDA) algorithm (Blei et al., 2003), which depends on the User-Topics probability density function (PDF) and the Topic-Words PDF. The user preference is simulated according to the 20-Newsgroups dataset (Lang, 1995) and it is learned by the LDA algorithm. The learned user preferences are clustered by the K–means algorithm for the users-to-

Nooh, H., Zhu, Z. and Ng, S.
Machine Learning Assisted Caching and Adaptive LDPC Coded Modulation for Next Generation Wireless Communications.
DOI: 10.5220/0009840500670076
In *Proceedings of the 17th International Joint Conference on e-Business and Telecommunications (ICETE 2020) - DCNET, OPTICS, SIGMAP and WINSYS*, pages 67-76
ISBN: 978-989-758-445-9

UAVs allocation. When the user preference is accurately predicted, useful data can be cached. If a user request is in the UAV's cached memory, it could be sent directly to the user from the UAV, without further requests to a remote BS. Thus, the user request delay is reduced.

Low Density Parity Check (LDPC) codes (Gallager, 1963; Guo, 2005) are powerful forward error correction schemes that have been widely investigated and are considered in the 5G standard. Adaptive coding and modulation (L. Hanzo, S. X. Ng and T. Keller, 2005) is another attractive transmission technology, where a high-rate channel code and a high-order modulation scheme are employed, for increasing the transmission rate, when the channel quality is good. By contrast, a low-rate channel code and a low-order modulation scheme are employed, for improving the transmission reliability, when the channel quality is poor. In this contribution, an Adaptive LDPC Coded Modulation (ALDPC-CM) scheme was investigated and utilized for the UAV-user communication link. The ALDPC-CM scheme could provide a near-capacity transmission rate for a given channel Signal-to-Noise-Ratio (SNR). Hence, a communication link with high SNR could lead to a lower transmission period (or transmission delay).

The rest of this paper is organized as follows. The caching model is investigated in Section 2, while our system model is detailed in Section 3. Our simulation results are discussed in Section 4, while our conclusions are summarized in Section 5.

2 CACHING MODEL

In this section, the Latent Dirichlet Allocation algorithm is outlined and the user preference model is presented.

2.1 Latent Dirichlet Allocation

Latent Dirichlet Allocation (LDA) is a generative probabilistic model (Blei et al., 2003) that characterizes the document generating process with the graphical model. The grey parameters shown in Fig. 1 are latent variables and cannot be observed. The remaining variables could be observed with the input data. LDA algorithm iteratively simulates the generating process and estimates the latent variables. The generated data is then evaluated using a cost function. Additionally, the latent variables are iteratively optimized based on the cost function. Once the model has converged, it can be used to predict the content of future user requests.

The LDA model is able to reveal the topic composition of a document and the word probability that is related to each topic. It classifies the new document into different classes and predicts the new words. It is useful for our system since users that share the same interest may be gathering around the same geographical location under specific application scenarios. LDA is a Bag-of-Words (BoW) model that neglects the order of words in the document. In our case, the order of user requests is not important. Hence, the LDA algorithm can be employed to perform user request prediction. More explicitly, LDA is composed of document generation and parameter estimation, where its graphical model is shown in Fig. 1. The meaning of symbols used in Fig. 1 are presented in Table 1. In our context, a 'document' represents the 'content requested by a user'.

We assume that there are a total of $|\mathcal{T}| = N_T$ topics, e.g. cars, movies, weather, news, etc, and they are controlled by Dirichlet distribution $\mathrm{Dir}(\alpha)$. For each user, their interest topics can be regarded as independent identical distributed (i.i.d) random variables sampled from $Dir(\alpha)$. For example, Bob (Bob $\in \mathcal{C}$) is interested in 40% of news, 10% of cars, 50% of movies, and 0% for the rest. Then, we can compute the User-Topics distribution of Bob, $\theta^{(d)}$. On the other hand, we have Topic-Contents distribution of each topic ϕ^t for $t \in \mathcal{T}$. These distributions are controlled by another Dirichlet distribution $\mathrm{Dir}(\beta)$. Thus, we can sample from θ^d and ϕ^t to generate a content $w_i^{(d)}$ for Bob. We continue to do this until we have generated all N_d contents for each $d \in \mathcal{C}$. Likewise, this model can generate contents for each user. In general, the probability that a word blank w is filled by a term t is given by:

$$p(w=t) \quad = \quad \sum_k \phi^{(k)}(w=t|z=k)\theta^{(d)}(z=k), \quad (1)$$

where $\sum_k \theta^{(d)}(z=k) = 1$.

2.2 User Preference Model

To simulate the user request behaviour and to generate the related distributions, we performed an LDA clustering over a text dataset called 20-Newsgroups dataset, which was first introduced in (Lang, 1995). It is a popular dataset for experiments in text applications, which is composed of 20 groups of news. Fig. 2(a) shows the main topics of the dataset. We need to preprocess the dataset to filter out the stop words before the LDA algorithm is employed. Then, we extract $n_w = 1000$ significant words from the dataset to compose a dictionary. Fig. 2(b) shows the preprocessing of the dataset. Hence, once we

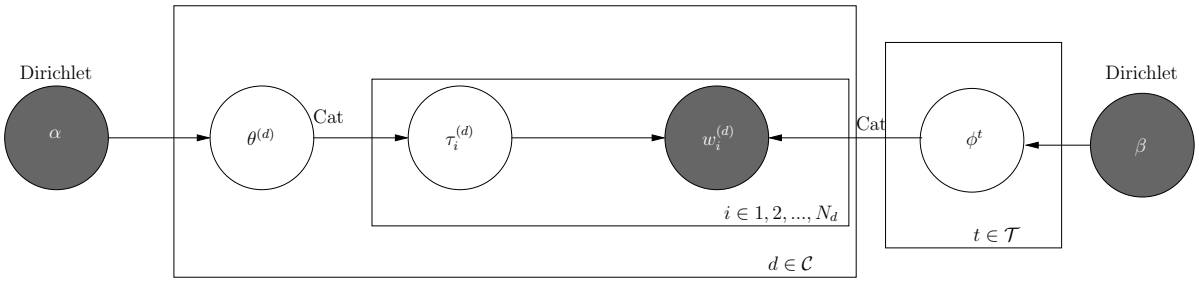

Figure 1: Graphical notation of the LDA algorithm. Each box in the diagram is a 'for' loop. From left to right: Dir(α) is a Dirichlet distribution with parameter α, it generates the topic distribution for each document; $\theta^{(d)}$ is sampled from Dir(α) and it represents the topics associated with each document. We then sample from $\theta^{(d)}$ to get a topic $\tau_i^{(d)}$ for the word $w_i^{(d)}$. From right to left: the words associated with each topic ϕ^t is sampled from another Dirichlet distribution with parameter β; we can then generate the word $w_i^{(d)}$ according to the sampled topic $\tau_i^{(d)}$ and the word distribution ϕ^t. Note that the grey circle represents the variables that are latent, N_d is the word count of the d-th document. $\mathcal{C}$ is the category of the documents and $\mathcal{T}$ is the set of topics.

Table 1: Symbol meaning of the LDA algorithm shown in Fig. 1.

Symbols	Contents Generation	Documents Generation
$\mathcal{C}$	User groups	Document categories
$d \in \mathcal{C}$	User	Document
$i \in 1, 2, ..., N_d$	i-th content blank of d	i-th word blank of d
Dir(α)	Generate User-Topics distributions	Generate Document-Topics distributions
Dir(β)	Generate Topic-Contents distributions	Generate Topic-Words distributions
$\theta^{(d)}$	User d's User-Topics distribution	Document d's Document-Topics distribution
$\tau_i^{(d)}$	i-th content blank's topic of d	i-th word blank's topic of d
ϕ^t	Topic t's Topic-Contents PDF	Topic t's Topic-Words PDF
$w_i^{(d)}$	i-th content of d	i-th word of d
$\mathcal{W}$	Contents Space, $w \in \mathcal{W}$	Dictionary, $w \in \mathcal{W}$

have finished the transform, we should have a $n_d \times n_w$ sparse matrix, which is 11314×1000 for this specific case. The sparse matrix is then input to the LDA algorithm.

We consider $N_u = 100$ users, $N_t = 4$ topics and $N_w = 100$ words (contents), as well as $N_d = 4$ UAVs to provide services to the users. The parameters α and β for Dirichlet distribution are generated based on the 20-Newsgroups dataset. We assign a Topic–Contents PDF for each topic, and a User–Topics PDF for each user. Fig. 3(a) shows the Topic–Contents PDFs. It is clear from Fig. 3(a) that different topics share distinct top five words, which are marked with red points. Fig. 3(b) shows the topic distribution for the first 20 users. As can be seen from Fig. 3(b), some users have a dominant topic amongst the four topics.

The preferred contents by each user may be different. The user preference is determined by the User-Topic Probability Density Function (UT-PDF) and Topic-Content Probability Density Function (TCPDF). For $N_u = 100$ users we have 200 PDFs as parameters to characterize the user preference. Again, these parameters are generated according to the 20-Newsgroup dataset. Fig. 4 shows the user preference with their dominant topics.

K-means clustering is then performed to match each user to a UAV, in order to optimize the system QoS, which is characterized mathematically as a function of delay ($\tau_i, \quad i \in 1, 2, ..., N_u$). The delay function for the ith user is determined by two terms, namely the time to transmit the content to the user from the UAV (τ_i^t) and time to request the content (unavailable at the UAV) from the remote BS (τ_i^r). For a given request S_i, the transmit delay τ_i^t and request delay τ_i^r are given by Eq. (2) and Eq. (3), respectively.

$$\tau_i^t = f(SNR, S_i), \tag{2}$$

$$\tau_i^r = \begin{cases} 0 & S_i \in C_d \\ 1 & S_i \notin C_d \end{cases} \qquad d \in 1, 2, ..., N_d, \tag{3}$$

where C_d is the contents cached in UAV d, which is serving user i. For example, the request delay equals to zero if the UAV has the user request in its memory. Hence, the system delay for all users can be computed as:

$$\tau = \sum_{i=1}^{N_d} \left(\tau_i^t + \tau_i^r\right), \tag{4}$$

which is a function of the receive SNR and the requested content. Further analysis on this is carried out in Section 4.2.

(a) The groups of the 20 Newsgroups dataset. The dataset is composed of 20 newsgroups and they belong to 6 general topics. There are a total of $n_d = 11314$ documents in the dataset. Besides, some of the groups are highly related to each other (i.e., hardware for PC and MAC).

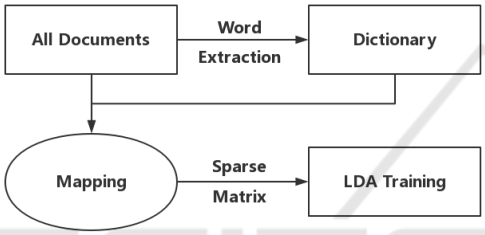

(b) The preprocessing of the input documents. We extract the first 1000 high frequency words as our dictionary. Then, we use this dictionary to transform each document into a sparse vector, where the value of its n-th element represents the number of repetitions of the n-th word in the dictionary.

Figure 2: Composition and preprocessing of the 20-Newsgroup dataset.

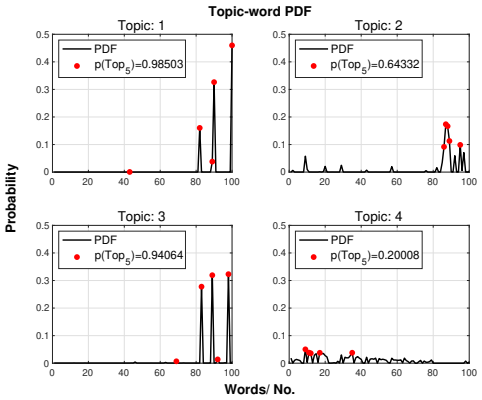

(a) Words distribution for all four topics. The top five frequent words are highlighted in red.

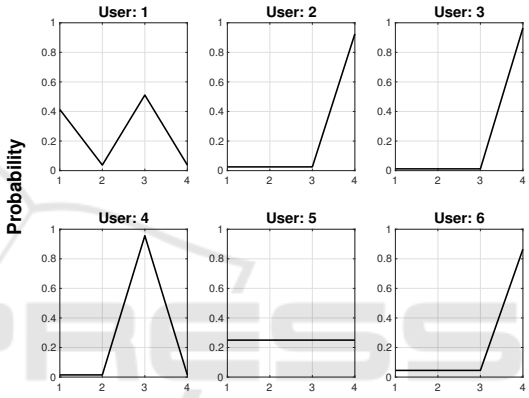

(b) Topic distribution for the first 6 users.

Figure 3: Generated users Topic–Contents PDFs and User–Topics PDFs. We assume $n_T = 4$ topics and $n_C = 100$ contents.

3 SYSTEM MODEL

3.1 Rician Fading Channel

The Rician fading channel models a dominant (non-variant) component amongst the multipath fading channel components (Goldsmith, 2005). This dominant component can be used to model the Line-of-Sight (LoS) link between the UAV and its user. The Rician PDF is given by:

$$p(r) = \frac{r}{\sigma^2} \exp\left(-\frac{A^2 + r^2}{2\sigma^2}\right) I_0 \frac{A_0}{\sigma^2}, \qquad (5)$$

where A is the peak amplitude of the dominant signal, I_0 is the zero-order modified Bessel function of the first kind, $K = \frac{A_0}{2\sigma^2}$ is the Rician factor representing the ratio of the dominant signal power to the multipath variance. As $K \to 0$ Eq. (5) approaches the Rayleigh PDF:

$$p(r) = \frac{r}{\sigma^2} \exp\left(-\frac{r^2}{2\sigma^2}\right), \qquad (6)$$

which is the commonly used model to describe the statistical time varying nature of the multipath fading channel without a dominant component. In a similar manner, as $K \to \infty$ The Rician PDF approaches the Gaussian distribution.

3.2 LDPC Codes

Low Density Parity Check (LDPC) codes (Gallager, 1963; D. J. C Mackay, and R. M. Neal, 1997) belong to the family of linear block codes, which are defined by a parity check matrix having M rows and N columns. The column and row weights are low compared to the dimension M and N of the parity check matrix H. Fig. 5 shows the bipartite graph (M. R. Tanner, 1981) representation of the parity check matrix.

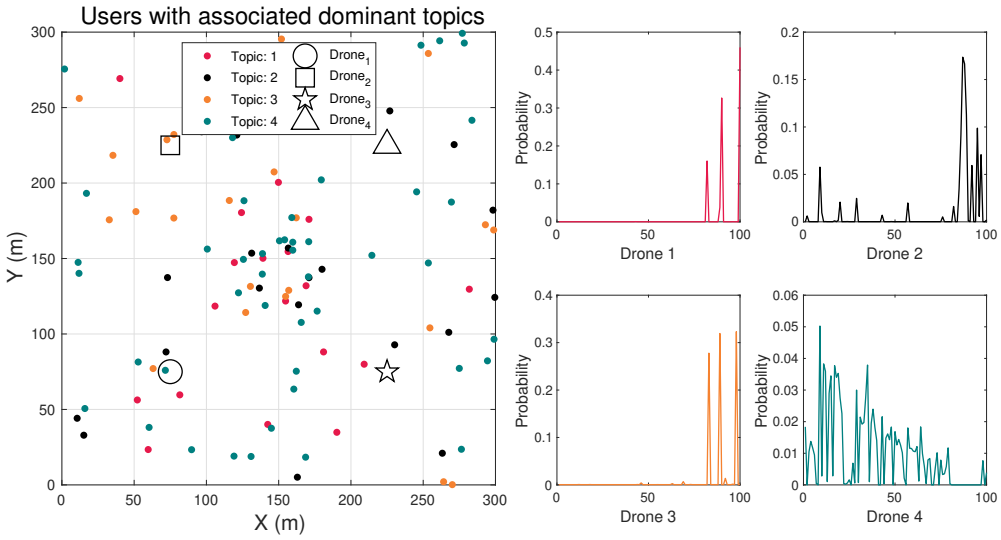

Figure 4: The primary model with user preference. $N_d = 4$ UAVs serving $N_u = 100$ users within a 300m×300m area.

This graph constitutes of two types of nodes, namely the *message nodes*, each of which corresponds to a column of the parity check matrix, and the *check nodes*, each of which corresponds to a row of the matrix. There are lines connecting these two types of nodes, and each connection corresponds to a non-zero entry in the parity check matrix of Fig. 5. For example, the non-zero entry at the bottom right corner of the parity check matrix in Fig. 5 corresponds to the connection between the 6^{th} node on the left and the 3^{rd} node on the right.

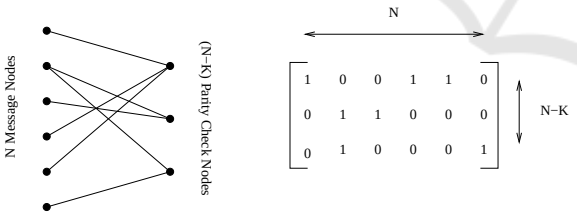

Figure 5: Bipartite graph representation of the parity check matrix.

The number of information bits encoded by an LDPC code is denoted by $K = N - M$, yielding a coding rate:

$$R_c = \frac{K}{N} \tag{7}$$

The modulation rate for an M-ary modulation is given by:

$$R_m = \log_2(M) \ . \tag{8}$$

R_m is the number of modulated bits per symbol, e.g. for BPSK, QPSK, and 8PSK, we have R_m equals to 1, 2 and 3 bits, respectively. Hence, the overall rate of the coded modulation scheme (or *information* bits per modulated symbol) can be computed as:

$$R = R_c \cdot R_m = \frac{K}{N} \cdot \log_2(M) \ . \tag{9}$$

3.3 Adaptive LDPC Coded Modulation

Fig. 6 shows the Bit Error Ratio (BER) versus SNR performance of an LDPC-coded 8PSK scheme, when communicating over Rician fading channels. Table 2 depicts the corresponding parameters. The size of the H is chosen to maintain a code rate of $R_c = 0.5$. As seen from Fig. 6, as the Rician factor K increases, the BER performance improves because the channel becomes more Gaussian like. When $K = 0$, the channel becomes a harsh Rayleigh fading channel. We have chosen a Rician factor of $K = 3$ for the rest of our simulations.

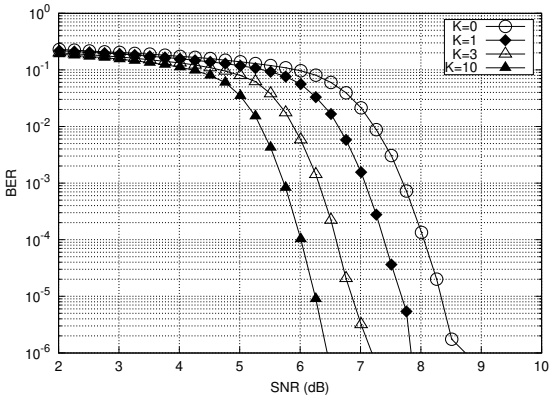

Figure 6: BER versus SNR performance of LDPC-coded 8PSK scheme, when communicating over Rician fading channels having a Rician factor of $K = \{0, 1, 3, 10\}$.

Table 2: LDPC coding parameters used in Fig. 6.

Parameter	Value
Maximum decoding iterations	15
Maximum Frame Size	100 000 bits
Column Weight	3
H Matrix Size	2400×1200

In order for a range of data rates to be supported in the UAV system the rate can be manipulated such that each modulation supports a throughput value progressively higher than the previous scheme, as outlined below. More specifically, the proposed ALDPC-CM scheme supports 8 transmission modes as detailed in Table 3. The BER versus SNR performance of these LDPC coded modulation schemes have been simulated when communicating over AWGN channel (Fig. 7), Rician fading channel (Fig. 8) and Rayleigh fading channels (Fig. 9).

Table 3: Parameters of ALDPC-CM modes.

Modulation	Coding Rate	Parity Check Matrix Size ($K \times N$)	Throughput (bits/symbol)
BPSK	0.5	2100×4200	0.5
4QAM	0.5	2100×4200	1
8PSK	2/3	2100×3150	2
16QAM	3/4	2100×2800	3
32QAM	4/5	2100×2625	4
64QAM	5/6	2100×2520	5
128QAM	6/7	2100×2450	6
256QAM	7/8	2100×2400	7

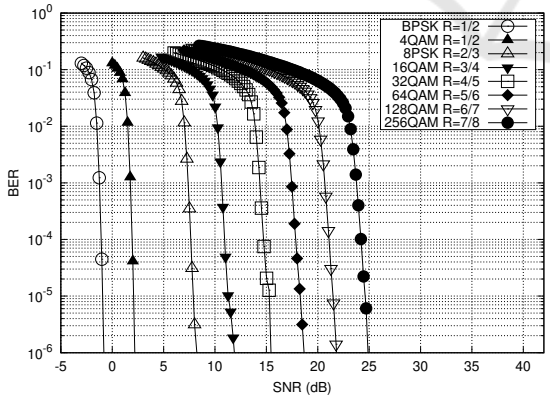

Figure 7: BER performance of LDPC coded modulation when communicating over AWGN channels $K = \infty$.

Based on the BER curves in Fig. 7, Fig. 8 and Fig. 9, we extract the SNR thresholds for each of these LDPC coded modulation schemes at a target BER of 10^{-4}, which are tabulated in in Table 4. The results displayed on Table 4 are inline with our expectations based on our prior knowledge of the nature of the respective channels. The AWGN channel

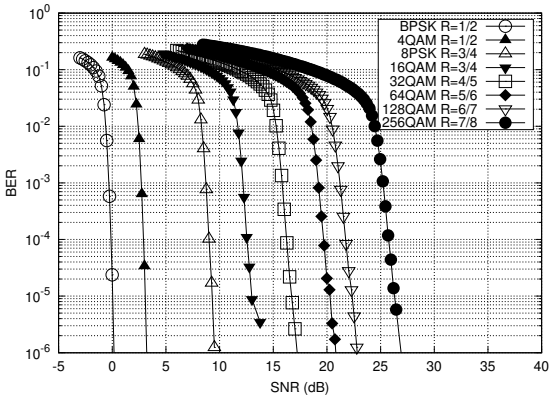

Figure 8: BER performance of LDPC coded modulation when communicating over Rician fading channels $K = 3$.

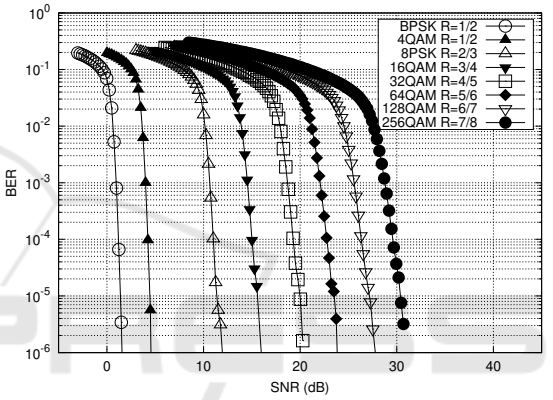

Figure 9: BER performance of LDPC coded modulation when communicating over Rayleigh fading channels $K = 0$.

Table 4: SNR thresholds at BER = 10^{-4} for various LDPC CM schemes. The perfect coding scheme is based on the channel capacity of the 256QAM scheme.

Modulation	Perfect Coding (dB)	AWGN (dB)	Rician, K=3 (dB)	Rayleigh (dB)
BPSK	-3	-0.899	-0.236	1.029
4QAM	1	2.092	2.775	4.043
8PSK	6	7.538	8.810	10.829
16QAM	9	10.806	12.332	14.847
32QAM	13	14.564	16.080	18.778
64QAM	16	17.568	19.346	22.413
128QAM	20	20.858	21.418	25.983
256QAM	23	24.026	25.556	29.200

is the best case for all the LDPC coded modulation schemes followed by the Rician fading channel and the Rayleigh fading channel. It is also worth pointing out that the Rician fading channel ($K = 3$) is closer to the ideal case of the AWGN channel than the worst case (Rayleigh fading channel) across all schemes. Fig. 10 shows a visual presentation of the data presented in Tables 3 and 4. As seen in Fig. 10, when actual coding (which has a discrete coding rate) is used,

the throughput has a staircase like curve. This is because when the received SNR is between two thresholds, a lower coded modulation mode is activated. For example, when the received SNR is above 12.332 dB but below 16.080 dB (see Table 4), LDPC-16QAM will be invoked when communicating over the Rician fading channels. Hence, a constant throughput of 3 bits/symbol (see Table 3) will be yielded for a received SNR that is above 12.332 dB but below 16.080 dB.

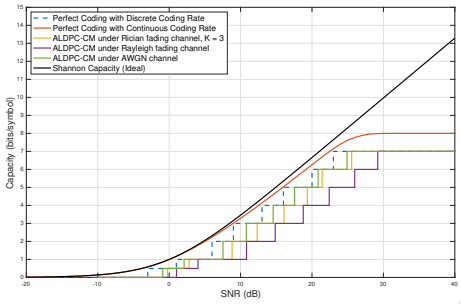

Figure 10: Capacity or throughput versus SNR curves of the ALDPC-CM scheme in comparison with theoretical limits. The Shannon capacity and the two 'Perfect Coding' schemes are based on AWGN channels.

4 RESULTS AND DISCUSSIONS

A simulator was created to investigate the overall system performance of the proposed UAV based scheme, incorporating machine learning assisted caching and ALDPC-CM aided transmission. The mobile users are served by UAVs, while the UAVs are connected wirelessly to a Base Station (BS).

The user preferences are estimated by the LDA algorithm, which classifies the information (word by word) into a set of topics. The users are then clustered into N_d groups and each user is allocated to a UAV. This last step is carried out using the K–means clustering algorithm. Three user-UAV allocation criteria were considered:

1. *max-snr*: allocate user to the UAV that would give the highest received SNR for minimizing the transmission delay.
2. *caching-efficiency*: allocate user to the UAV that is likely to have the requested content, for minimizing the request delay.
3. *min-delay*: allocate user to the UAV that would minimize the overall delay (the sum of both transmission and request delay).

4.1 Caching Efficiency

In this section, we investigate the performance of LDA based caching technique in comparison to a random caching benchmark scheme. For most scenarios, only a limited amount of historical user requests can be accessed. Besides, it is also important to provide immediate QoS to users once the connection is established. Hence, the system delay under limited historical requests is a significant performance indicator. Here, we assume that each user is allocated to a UAV that has a link with the highest received SNR (i.e. *max-snr* criteria). Then, we only examine the effect of different caching strategies. A perfect coding scheme with continuous coding rate is assumed in this subsection.

The simulation results for LDA based caching and random caching with different historical request sizes are shown in Fig. 11(a), when the UAV's memory size is 50% of the total data (i.e. $|\mathcal{C}_d| = 50$). It should be noticed that the x-axis in Fig. 11(a), which is the size of the historical requests, represents the number of past requests from each user. Not surprisingly the caching efficiency is around 50% for the random caching strategy. As shown in Fig. 11(a), the LDA based approach achieves above 90% caching efficiency after only 5 historical requests.

Fig. 11(b) shows the influence of both memory size and the number of historical requests. It can be observed from Fig. 11(b) that the memory size is more significant than the number of historical requests, when considering the caching efficiency. This is because the LDA algorithm learns user preferences relatively fast when the memory size is big, as shown in Fig. 11(a). We have shown that the LDA based caching scheme is significantly more efficient compared to the random caching method. The convergence speed of the LDA algorithm is also fast, especially when the memory size is big. Having considered the ideal case with perfect coding here, we will now investigate the performance of the ALDPC-CM based scheme in the following section.

4.2 Overall Delay

The simulation parameters used in this section are given in Table 5. The ALDPC-CM scheme supports the 8 transmission modes detailed in Table 3, which have SNR thresholds shown in Table 4. Table 6 shows the throughput achieved for each coded modulation mode. Additionally, if the received SNR is lower than the SNR threshold of the lowest mode (BPSK), then no transmission (No Tx) will happen. By contrast, when the received SNR is higher than the highest

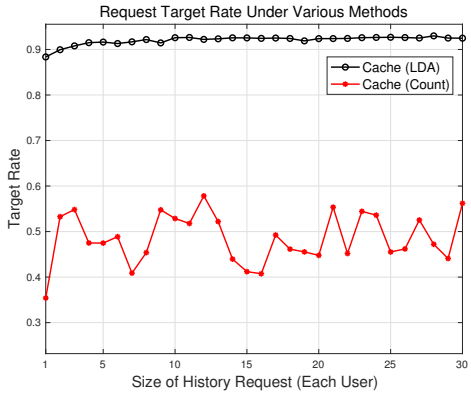

(a) Caching efficiency simulation of LDA based and random caching strategies under varying size of historical requests. The system has $n_U = 100$ users, $n_D = 4$ UAVs, $n_C = 100$ contents, and $n_T = 4$ topics. A total of $|\mathcal{C}_d| = 50$ contents can be cached for each UAV.

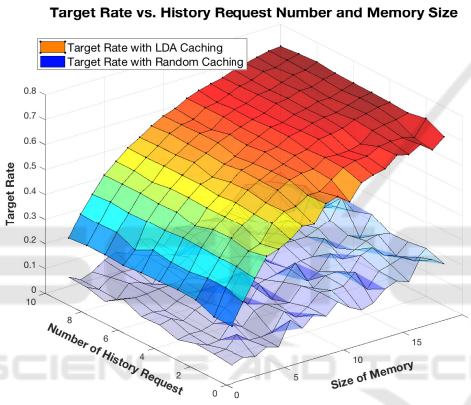

(b) Caching efficiency simulation of LDA based and random caching strategies under varying size of historical requests and a range of memory sizes.

Figure 11: Caching efficiency simulation based on perfect coding scheme that has continuous coding rate.

mode (256QAM), then a throughput of 7 bits/symbol will be supported, as illustrated in Table 6.

Fig. 12 shows the instantaneous delay and mean delay of the ALDPC-CM based scheme, for the three user-UAV allocation criteria considered. The user-UAV allocation constitutes a trade-off between available resources. As seen in Fig. 12, minimizing the transmission delay (max-snr criteria) would give a lower mean delay compared to minimizing the request delay (caching-efficiency criteria). Hence, the transmission delay is more dominant than the request delay in our system. Furthermore, the min-delay criteria gives the lowest mean delay as expected. However, this would require additional computation/overhead for calculating the transmission delay and the request delay.

Table 5: Simulation Parameters.

Parameter	Value
No. of UAVs	4
No. of users	50
Total contents, n_C	100
Area served	300 m^2
Drone/UAV height	30 m
Noise PSD	-85 dBm
Signal bandwidth	20 MHz
Carrier Frequency	2 GHz
UAV's memory size, $\|\mathcal{C}_d\|$	50
UAV-BS Request delay	2 ms
Maximum user speed	15 m/s
Coded Modulation scheme	ALDPC-CM

Table 6: Data rates for various LDPC-CM schemes.

Capacity Interval (bits/symbol)	Modulation	Coding Rate	Throughput (bits/symbol)
[−∞,0.5]	No Tx	0	0
[0.5,1]	BPSK	0.5	0.5
[1,2]	4QAM	0.5	1
[2,3]	8PSK	2/3	2
[3,4]	16QAM	3/4	3
[4,5]	32QAM	4/5	4
[5,6]	64QAM	5/6	5
[6,7]	128QAM	6/7	6
[7,+∞]	256QAM	7/8	7

Fig. 13 shows the instantaneous delay comparison for the ALDPC-CM based transmission scheme when considering the three user-UAV allocation criteria. The max-snr criteria may be considered as a good tradeoff in terms of performance and complexity. Table 7 depicts the mean delay values associated with the instantaneous delay plots shown in Fig. 13 under each criterion. The practical ALDPC-CM based scheme only invoked an additional mean delay of $1.32 - 1.27 = 0.05$ ms compared to the ideal perfect coding based scheme when the min-delay criteria is considered, as shown in Table 7.

Table 7: Mean delay comparison over 101 frames.

Criterion	Mean Delay (ms), ALDPC-CM	Mean Delay (ms), Perfect Coding
max-snr	2.02	1.27
min-delay	1.32	1.27
caching-efficiency	3.16	2.84

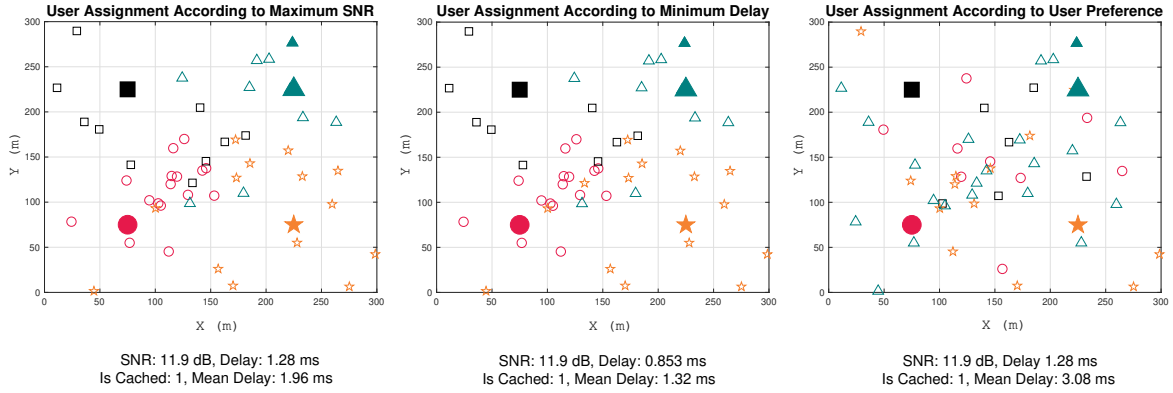

Figure 12: An instance of the moving user allocation process under three allocation criteria. The four UAVs are represented by the four filled-markers, while users allocated to the UAV are denoted by the blank-markers of the same shape and color.

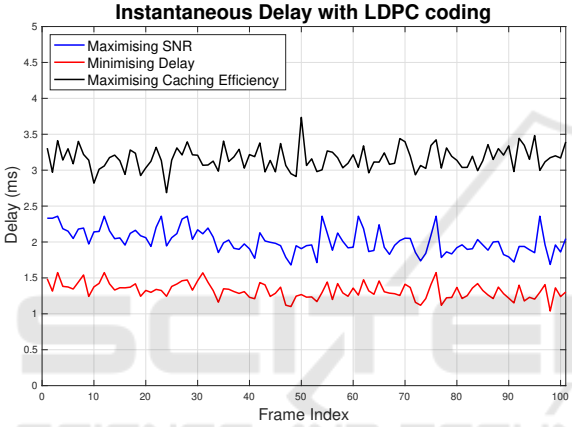

Figure 13: Instantaneous delay comparison for the ALDPC-CM based transmission scheme when considering the three user-UAV criteria.

5 CONCLUSIONS AND FUTURE WORK

In this contribution, we have proposed an LDA based machine learning technique for predicting user requests, which is then investigated for improving the caching efficiency of UAVs. It was evidenced in Fig. 11 that the LDA based caching significantly outperformed the random caching method, where above 90% caching efficiency can be achieved after a short training based on 5 historical user requests.

We have also implemented an ALDPC-CM scheme that can support 8 transmission modes on top of the no transmission mode, as outlined in Table 6. The Rician fading channel having a Rician factor of $K = 3$ was invoked for modeling the LoS link between the UAV and its serving users. A range of simulations were done for computing the BER versus SNR curves of the various LDPC-CM schemes as shown in Fig. 7, Fig. 8 and Fig. 9. An adaptive scheme was then created for maintaining a BER of $\leq 10^{-4}$ while increasing the link throughput as the channel SNR improves, as depicted in Fig. 10.

After the caching technique and the link-level transmission were implemented, the K–means algorithm was then utilized for allocating all users to the UAVs. Three allocation criteria were considered, where the max-snr criterion aims to minimize the transmission delay, the caching-efficiency criterion aims to minimize the request delay and the min-delay criterion aims to minimize the overall delay. We found that the min-delay criterion would give the lowest mean delay, while the max-snr criteria is a good tradeoff when considering the achievable performance and required complexity, as shown in Fig. 13. The proposed practical ALDPC-CM based scheme performed very close to the ideal perfect coding scheme, as evidenced in Table 7.

For the future work, other machine learning models such as the Non-negative Matrix Factorization (NMF) should be comparatively analyzed against our LDA-based approach for caching optimization. Other channel coding schemes such as polar codes, trellis codes and space-time codes can also be utilized in the link-level transmission. Deep Learning and Reinforcement Learning techniques (Ha et al., 2019), (Bruno et al., 2014) could also be considered for improving the overall performance of the UAV based system.

REFERENCES

Americas, G. (2018). 5g ultra-reliable and low-latency communication (urllc) to digitize industries and unearth new use cases. White paper, 5G Americas.

Blei, D. M., Ng, A. Y., and Jordan, M. I. (2003). Latent

dirichlet allocation. *Journal of machine Learning research*, 3(Jan):993–1022.

Bruno, R., Masaracchia, A., and Passarella, A. (2014). Robust adaptive modulation and coding (amc) selection in lte systems using reinforcement learning. In *2014 IEEE 80th Vehicular Technology Conference (VTC2014-Fall)*, pages 1–6.

Chen, M., Challita, U., Saad, W., Yin, C., and Debbah, M. (2017). Machine learning for wireless networks with artificial intelligence: A tutorial on neural networks. *arXiv preprint arXiv:1710.02913*.

D. J. C Mackay, and R. M. Neal (1997). Near shannon limit performance of low density parity check codes. *Electronics Letters*, 33(6):457–458.

Gallager, R. G. (1963). *Low Density Parity Check Codes*. PhD thesis, M.I.T, United States.

Goldsmith, A. (2005). *Wireless communications*. Cambridge university press.

Guo, F. (2005). *Low Density Parity Check Coding*. PhD thesis, University of Southampton, United Kingdom.

Ha, C., You, Y., and Song, H. (2019). Machine learning model for adaptive modulation of multi-stream in mimo-ofdm system. *IEEE Access*, 7:5141–5152.

L. Hanzo, S. X. Ng and T. Keller (2005). *Quadrature Amplitude Modulation : From Basics to Adaptive Trellis-Coded, Turbo-Equalised and Space-Time Coded OFDM, CDMA and MC-CDMA Systems*. IEEE Press.

Lang, K. (1995). Newsweeder: Learning to filter netnews. In *Proceedings of the Twelfth International Conference on Machine Learning*, pages 331–339.

M. R. Tanner (1981). A recursive approach to low complexity codes. *IEEE Transactions on Information Theory*, 27(5).

Merwaday, A. and Guvenc, I. (2015). Uav assisted heterogeneous networks for public safety communications. In *Wireless Communications and Networking Conference Workshops (WCNCW), 2015 IEEE*, pages 329–334. IEEE.

Valavanis, K. P. and Vachtsevanos, G. J. (2014). *Handbook of Unmanned Aerial Vehicles*. Springer Publishing Company, Incorporated.

Wang, S., Zhang, X., Zhang, Y., Wang, L., Yang, J., and Wang, W. (2017). A survey on mobile edge networks: Convergence of computing, caching and communications. *IEEE Access*, 5:6757–6779.

Zeng, Y., Zhang, R., and Lim, T. J. (2016). Wireless communications with unmanned aerial vehicles: opportunities and challenges. *arXiv preprint arXiv:1602.03602*.